# One-way spatial integration of hyperbolic equations

Aaron Towne *, Tim Colonius

*California Institute of Technology, Pasadena, CA 91125, USA*

ARTICLE INFO

ABSTRACT

In this paper, we develop and demonstrate a method for constructing well-posed one-way approximations of linear hyperbolic systems. We use a semi-discrete approach that allows the method to be applied to a wider class of problems than existing methods based on analytical factorization of idealized dispersion relations. After establishing the existence of an exact one-way equation for systems whose coefficients do not vary along the axis of integration, efficient approximations of the one-way operator are constructed by generalizing techniques previously used to create nonreflecting boundary conditions. When physically justified, the method can be applied to systems with slowly varying coefficients in the direction of integration. To demonstrate the accuracy and computational efficiency of the approach, the method is applied to model problems in acoustics and fluid dynamics via the linearized Euler equations; in particular we consider the scattering of sound waves from a vortex and the evolution of hydrodynamic wavepackets in a spatially evolving jet. The latter problem shows the potential of the method to offer a systematic, convergent alternative to ad hoc regularizations such as the parabolized stability equations.

© 2015 Published by Elsevier Inc.

## 1. Introduction

Many physical phenomena can be modeled by systems of linear hyperbolic partial differential equations. A defining characteristic of hyperbolic systems is that their solutions are comprised of waves that propagate at finite speeds. The well-posed solution of these equations on a finite computational domain takes the form of either an initial boundary value problem in the time domain or an elliptic boundary value problem if the equations are transformed into the frequency domain. In either case, incoming waves must be specified at the boundaries.

In some situations, the solution is dominated by waves that propagate in one direction. We call these waves rightgoing and the waves that propagate in the opposite direction leftgoing. Approximate one-way equations are often sought to represent the rightgoing waves. These one-way equations, also known as parabolized or parabolic equations, are valuable because they can be rapidly solved in the frequency domain by spatial integration in the direction of wave propagation. For the spatial march to be accurate and well-posed, the one-way equation must approximate the same rightgoing waves as the original hyperbolic equation but not support any leftgoing waves. If support for the leftgoing waves is not properly removed, decaying leftgoing waves are wrongly interpreted as growing downstream waves, causing instability in the spatial march.

One-way equations have been formally derived for various wave equations. Most one-way wave equations are derived by factoring the dispersion relation in Fourier–Laplace space. Two factors are obtained – one representing rightgoing waves

---

* Corresponding author.
 *E-mail addresses:* atowne@caltech.edu (A. Towne), colonius@caltech.edu (T. Colonius).

and one representing leftgoing waves. A one-way wave equation is obtained by only retaining the rightgoing branch. The resulting equation contains a square root involving the Fourier–Laplace variables, and the inverse transform of this term results in a nonlocal integro-differential equation. Computationally efficient one-way wave equations can be obtained by localizing the operator using rational approximations of the square root [1]. Early methods involved approximations at a fixed low order [2,3], while subsequent versions generalized this idea to arbitrarily high-order approximations. The accuracy and well-posedness of different approximations have been extensively studied [4,5]. One-way wave equations are routinely used to study geophysical migration [6,7] and underwater acoustics [8,9], and, when transformed back to the time domain, can be used as approximate nonreflecting boundary conditions [10,11].

These methods are very efficient and accurate for simple wave equations but degenerate quickly in more complicated situations because of their dependence on the factorization of the equations in Fourier–Laplace space, which, for example, is not possible for equations whose eigenvalues cannot be written down analytically. It is therefore not straightforward to apply these techniques to general hyperbolic systems. Guddati [12] developed a method for the acoustic and elastic wave equations that does not depend on this factorization. His method shares some qualitative similarities to the scheme we propose in this paper, but it has not been extended beyond wave equations.

The linearized Euler and Navier–Stokes equations can be spatially integrated using an ad hoc generalization of linear stability theory called the parabolized stability equations (PSE) [13]. PSE is designed to track the one-way spatial evolution of a single rightgoing wave, usually the most spatially amplified wave supported by the system. The wavelength and growth-rate of this wave are assumed to be slowly-varying. Instead of formally deriving a one-way operator, PSE achieves a stable spatial march by numerically damping all leftgoing waves, either by using an implicit axial discretization along with a restriction on the *minimum* step size [14] or by explicitly adding damping terms to the equations [15]. This damping prevents the leftgoing waves from destabilizing the spatial march, but also has the unintended consequence of damping and distorting, to differing degrees, all of the rightgoing waves.

PSE has been used extensively to study instability waves in slowly-spreading shear-flows. It is often the case that the near-field solutions of these equations are dominated by a single amplifying rightgoing wave related to classic instability modes of the Orr–Sommerfeld operator. This wave can be calculated very efficiently with reasonable accuracy using PSE. On the other hand, other rightgoing waves supported by the Euler equations, for example rightgoing acoustic waves, are not properly captured by PSE because of the aforementioned damping.

A number of other spatial marching methods have been developed for solving the Euler and Navier–Stokes equations that are collectively known as reduced or parabolized Navier–Stokes equations. After neglecting viscous terms in the parabolization direction, leftgoing acoustic waves are eliminated by special treatment of the streamwise pressure gradient. A number of variations exist in which this term is treated differently, ranging from neglecting it partially [16] or entirely [17] to prescribing it based on experimental data [17] or empirical approximations. Classical boundary layer equations fall into this category.

In this paper, we describe and demonstrate a new technique for developing accurate one-way approximations of linear hyperbolic systems. Our method formally removes support for leftgoing waves from the equations without analytically factorizing the dispersion relation, resulting in well-posed equations that can be solved by spatial marching without the need for numerical damping. As a result, the rightgoing waves can be accurately captured for systems in which the leftgoing waves are unimportant. In Section 2, we first derive exact one-way equations based on concepts related to the well-posedness of hyperbolic boundary value problems and then show how the exact equations can be efficiently approximated using techniques that were originally developed for generating high-order nonreflecting boundary conditions. The method is applied to the Euler equations in Section 3, and the accuracy and efficiency of the resulting one-way Euler equations is demonstrated in Section 4 using three example problems. Finally, we discuss possible improvements to the method and conclude the paper in Section 5.

## 2. Method

In this section, we formulate our parabolization method. First, we derive the spatial boundary value problem for a general hyperbolic system. Then, we derive an exact one-way equation for systems that are homogeneous along the axis of parabolization by identifying and eliminating leftgoing waves. The exact formulation is computationally expensive, so we next formulate efficient, well-posed approximations of the exact equations. We discuss the application of these methods to systems that vary along the axis of parabolization and finally compare the computational cost of the one-way equations to standard solution techniques.

### 2.1. Problem formulation

We begin with a system of linear, strongly hyperbolic partial differential equations

$$\frac{\partial q}{\partial t} + A(x, y)\frac{\partial q}{\partial x} + \sum_{j=1}^{d-1} B_j(x, y)\frac{\partial q}{\partial y_j} + C(x, y)q = 0. \tag{1}$$

Here, $x \in \mathbb{R}$ is the axis along which we will parabolize the equations, $y = \{y_1, \ldots, y_{d-1}\} \in \mathbb{R}^{d-1}$ are additional, transverse spatial dimensions, and $d$ is the total spatial dimensionality of the problem. The coefficients $A$, $B_j$, $C \in \mathbb{C}^{N_q \times N_q}$ are smooth matrix functions of $x$ and $y$ and do not depend on $t$. The vector $q = q(x, y, t) \in \mathbb{C}^{N_q}$ is the solution to be determined.

We discretize equation (1) in the transverse directions using a total of $N_y$ degrees of freedom. Standard finite difference discretizations are used in the example problems presented in Section 4, but in principle any collocation method could be used. We represent the discrete analog of each continuous variable and operator with a bold variable of the same name. The semi-discrete approximation of equation (1) can then be written

$$\frac{\partial \boldsymbol{q}}{\partial t} + \boldsymbol{A}(x)\frac{\partial \boldsymbol{q}}{\partial x} + \boldsymbol{B}(x)\boldsymbol{q} = 0, \tag{2}$$

where $\boldsymbol{B} = \sum_{j=1}^{d-1} \boldsymbol{B}_j \boldsymbol{D}_j + \boldsymbol{C}$ and the matrix $\boldsymbol{D}_j$ approximates the derivative $\frac{\partial}{\partial y_j}$. At this point, transverse boundary conditions must also be incorporated into $\boldsymbol{B}$. It is important that these boundary conditions do not alter the structure of $\boldsymbol{A}$. Common options such as damping layers, perfectly matched layers, and characteristic boundary conditions satisfy this requirement.

Equation (2) is a one-dimensional strongly hyperbolic system. In other words, $\boldsymbol{A}$ is diagonalizable and has real eigenvalues. This follows from the fact that the entries of $\boldsymbol{A}$ are a discrete sampling of the continuous matrix $A$. Specifically, $\boldsymbol{A}$ can be written as a block-diagonal matrix, where each block contains the matrix $A$ evaluated at one of the collocation points. This structure guarantees that $\boldsymbol{A}$ is diagonalizable and that its eigenvalues are real, since they are precisely the eigenvalues of $A$ at the collocation points.

In the preceding development, equation (2) inherited strong hyperbolicity from equation (1). This is not, however, the only way to arrive at a system equivalent to equation (2). For example, higher order $y$ derivatives could be added to equation (1), destroying its hyperbolicity, without destroying the hyperbolicity of equation (2). The method described in the remainder of this paper can be applied to any linear, one-dimensional, strongly hyperbolic equation, regardless of its origin.

For simplicity, we restrict our attention to the case in which $\boldsymbol{A}$ is invertible for all $x$. This restriction is not necessary but simplifies the discussion. We treat the case where $\boldsymbol{A}$ is singular in Appendix A. Under this assumption, the number of positive and negative eigenvalues of $\boldsymbol{A}$ is fixed for all $x$, and we denote these quantities as $N_+$ and $N_-$, respectively. The total size of the semi-discrete system is $N = N_q N_y = N_+ + N_-$.

It proves useful to work with the characteristic variables of equation (2). Since $\boldsymbol{A}$ is diagonalizable, there exists a transformation $\boldsymbol{T}(x)$ such that

$$\boldsymbol{T}\boldsymbol{A}\boldsymbol{T}^{-1} = \tilde{\boldsymbol{A}} = \begin{bmatrix} \tilde{\boldsymbol{A}}_{++} & \boldsymbol{0} \\ \boldsymbol{0} & \tilde{\boldsymbol{A}}_{--} \end{bmatrix}, \tag{3}$$

where $\tilde{\boldsymbol{A}}_{++} \in \mathbb{R}^{N_+ \times N_+} > 0$, $\tilde{\boldsymbol{A}}_{--} \in \mathbb{R}^{N_- \times N_-} < 0$, and $\tilde{\boldsymbol{A}}$ are diagonal matrices. The diagonal entries of $\tilde{\boldsymbol{A}}_{++}$ and $\tilde{\boldsymbol{A}}_{--}$ are precisely the positive and negative eigenvalues of $\boldsymbol{A}$, respectively. The transformation $\boldsymbol{T}$ is known analytically since it is the discretization of the matrix $T$ that diagonalizes $A$.

The characteristic variables of equation (2) are then $\boldsymbol{\phi}(x, t) = \boldsymbol{T}(x)\boldsymbol{q}(x, t)$, and can be separated into positive and negative parts based on the positive and negative blocks of $\boldsymbol{A}$:

$$\boldsymbol{\phi} = \left\{ \begin{array}{c} \boldsymbol{\phi}_+ \\ \boldsymbol{\phi}_- \end{array} \right\} \tag{4}$$

with $\boldsymbol{\phi}_+ \in \mathbb{R}^{N_+}$ and $\boldsymbol{\phi}_- \in \mathbb{R}^{N_-}$. In terms of the characteristic variables, equation (2) becomes

$$\frac{\partial \boldsymbol{\phi}}{\partial t} + \tilde{\boldsymbol{A}}(x)\frac{\partial \boldsymbol{\phi}}{\partial x} + \tilde{\boldsymbol{B}}(x)\boldsymbol{\phi} = \boldsymbol{0}, \tag{5}$$

where $\tilde{\boldsymbol{B}} = \boldsymbol{T}\boldsymbol{B}\boldsymbol{T}^{-1} + \tilde{\boldsymbol{A}}\boldsymbol{T}\frac{d\boldsymbol{T}^{-1}}{dx}$.

Since we wish to obtain a one-way equation in the frequency domain, we proceed by applying a Laplace transform in time to equation (5), giving

$$s\hat{\boldsymbol{\phi}} + \tilde{\boldsymbol{A}}(x)\frac{\partial \hat{\boldsymbol{\phi}}}{\partial x} + \tilde{\boldsymbol{B}}(x)\hat{\boldsymbol{\phi}} = 0, \tag{6}$$

where $\hat{\boldsymbol{\phi}}(x, s)$ is the Laplace transform of $\boldsymbol{\phi}(x, t)$ and $s = \eta - i\omega$ $(\eta, \omega \in \mathbb{R})$ is the Laplace dual of $t$. We have assumed zero initial conditions, but that is unimportant since we are only interested in the long-time stationary behavior of the solution. We will ultimately take $\eta = 0$ and set $\omega$ to a particular value to obtain the stationary solution at that frequency, but keeping the possibility of non-zero $\eta$ will help us distinguish between upstream and downstream solutions of equation (5).

Solving equation (6) for $x$-derivatives gives

$$\frac{d\hat{\boldsymbol{\phi}}}{dx} = \boldsymbol{M}(x, s)\hat{\boldsymbol{\phi}} \tag{7}$$

with

$$\boldsymbol{M} = -\tilde{\boldsymbol{A}}^{-1} \left( s\boldsymbol{I} + \tilde{\boldsymbol{B}} \right). \tag{8}$$

It is useful to partition $\boldsymbol{M}$ into blocks according to the sizes of the positive and negative characteristic variables:

$$\frac{d}{dx} \left\{ \begin{array}{c} \hat{\boldsymbol{\phi}}_+ \\ \hat{\boldsymbol{\phi}}_- \end{array} \right\} = \left[ \begin{array}{cc} \boldsymbol{M}_{++} & \boldsymbol{M}_{+-} \\ \boldsymbol{M}_{-+} & \boldsymbol{M}_{--} \end{array} \right] \left\{ \begin{array}{c} \hat{\boldsymbol{\phi}}_+ \\ \hat{\boldsymbol{\phi}}_- \end{array} \right\}. \tag{9}$$

The size of each block is implied by the subscripts; for example, $\boldsymbol{M}_{+-} \in \mathbb{C}^{N_+ \times N_-}$. We will continue to use this convention throughout the paper.

## 2.2. Exact one-way equation

In this subsection, we show that there exists an exact parabolization of equation (7) for the special case in which $\boldsymbol{M}$ is not a function of $x$. The method will be extended to $x$-dependent operators in Section 2.4. We also assume that $\boldsymbol{M}$ is diagonalizable. It is shown in Appendix B that the methods developed for diagonalizable matrices can be applied without modification to systems in which $\boldsymbol{M}$ is defective.

The essential step in parabolizing equation (7) is distinguishing between its rightgoing and leftgoing solutions. Since equation (7) is uniform in $x$, its general solution is the summation of modes

$$\hat{\boldsymbol{\phi}}(x, s) = \sum_{k=1}^{N} \boldsymbol{v}_k(s) \boldsymbol{\psi}_k(x, s), \tag{10}$$

where each expansion coefficient $\boldsymbol{\psi}_k$ satisfies

$$\frac{d\boldsymbol{\psi}_k}{dx} = i\alpha_k(s) \boldsymbol{\psi}_k, \tag{11}$$

and each $(i\alpha_k, \boldsymbol{v}_k)$ is an eigenvalue-eigenvector pair of $\boldsymbol{M}$. We include the $i$ in our definition of the eigenvalue for consistency with the usual definition of spatial wave-numbers. The real and imaginary parts of $\alpha_k$ are related to the phase-speed and spatial growth rate of the mode.

The task at hand is to determine which of these modes are rightgoing and which are leftgoing, in terms of energy transfer. Briggs [18] developed a criterion for making this distinction: mode $k$ is rightgoing if

$$\lim_{\eta \to +\infty} \text{Im}\,[\alpha_k(s)] = +\infty \tag{12}$$

and leftgoing if

$$\lim_{\eta \to +\infty} \text{Im}\,[\alpha_k(s)] = -\infty. \tag{13}$$

Since $\boldsymbol{M}$ tends to the real diagonal matrix $-\eta\tilde{\boldsymbol{A}}^{-1}$ as $\eta \to +\infty$, it is clear that all of its eigenvalues will exhibit one of these two behaviors. Furthermore, based on the block structure of $\tilde{\boldsymbol{A}}$, there are exactly $N_+$ rightgoing modes and $N_-$ leftgoing modes. When applied to an operator obtained from a constant coefficient hyperbolic system such as equation (7), Briggs' criterion is consistent with well-posedness theory for hyperbolic systems as developed by Kreiss [19].

The exact parabolization of equation (7) is obtained by zeroing the leftgoing modes. That is, for each leftgoing mode, equation (11) is replaced with the condition

$$\boldsymbol{\psi}_k = 0. \tag{14}$$

This is exactly the same condition that is applied to each incoming mode in order to generate nonreflecting boundary conditions at an outflow. Indeed, our parabolization technique can be thought of as applying a nonreflecting outflow boundary condition not just at the boundary, but to the entire domain, since we wish to disallow leftgoing solutions everywhere to achieve a well-posed spatial march.

In order to write the one-way equation clearly and compactly, it is useful to write it in block matrix form. First, the expansion coefficients are arranged in a vector $\boldsymbol{\psi}$ such that the $N_+$ rightgoing modes appear first followed by the $N_-$ leftgoing modes:

$$\boldsymbol{\psi} = \left\{ \begin{array}{c} \boldsymbol{\psi}_+ \\ \boldsymbol{\psi}_- \end{array} \right\}. \tag{15}$$

Then equations (10)–(11) can be written in matrix form as

$$\hat{\boldsymbol{\phi}} = \boldsymbol{V}\boldsymbol{\psi} \quad \leftrightarrow \quad \boldsymbol{\psi} = \boldsymbol{U}\hat{\boldsymbol{\phi}} \tag{16}$$

and

$$\frac{d\boldsymbol{\psi}}{dx} = \boldsymbol{D}\boldsymbol{\psi}. \tag{17}$$

The columns of $\boldsymbol{V}$ are the right eigenvectors, the rows of $\boldsymbol{U} = \boldsymbol{V}^{-1}$ are the left eigenvectors, and the entries of the diagonal matrix $\boldsymbol{D}$ are the eigenvalues of $\boldsymbol{M}$, all ordered in the same way as $\boldsymbol{\psi}$, such that $\boldsymbol{M} = \boldsymbol{V}\boldsymbol{D}\boldsymbol{U}$.

We can also partition the matrices $\boldsymbol{V}$, $\boldsymbol{U}$, and $\boldsymbol{D}$ into blocks based on their association with the upstream and downstream expansion coefficients and the positive and negative characteristic variables. Specifically, we write

$$\begin{Bmatrix} \hat{\boldsymbol{\phi}}_+ \\ \hat{\boldsymbol{\phi}}_- \end{Bmatrix} = \begin{bmatrix} \boldsymbol{V}_{++} & \boldsymbol{V}_{+-} \\ \boldsymbol{V}_{-+} & \boldsymbol{V}_{--} \end{bmatrix} \begin{Bmatrix} \boldsymbol{\psi}_+ \\ \boldsymbol{\psi}_- \end{Bmatrix}, \tag{18}$$

$$\begin{Bmatrix} \boldsymbol{\psi}_+ \\ \boldsymbol{\psi}_- \end{Bmatrix} = \begin{bmatrix} \boldsymbol{U}_{++} & \boldsymbol{U}_{+-} \\ \boldsymbol{U}_{-+} & \boldsymbol{U}_{--} \end{bmatrix} \begin{Bmatrix} \hat{\boldsymbol{\phi}}_+ \\ \hat{\boldsymbol{\phi}}_- \end{Bmatrix}, \tag{19}$$

and

$$\frac{d}{dx} \begin{Bmatrix} \boldsymbol{\psi}_+ \\ \boldsymbol{\psi}_- \end{Bmatrix} = \begin{bmatrix} \boldsymbol{D}_{++} & \boldsymbol{0} \\ \boldsymbol{0} & \boldsymbol{D}_{--} \end{bmatrix} \begin{Bmatrix} \boldsymbol{\psi}_+ \\ \boldsymbol{\psi}_- \end{Bmatrix}. \tag{20}$$

Recall that based on our ordering of $\boldsymbol{\psi}$, $\boldsymbol{D}_{++}$ contains the rightgoing eigenvalues and $\boldsymbol{D}_{--}$ contains the leftgoing eigenvalues. We make one additional assumption: that the matrices $\boldsymbol{U}_{++}$, $\boldsymbol{U}_{--}$, $\boldsymbol{V}_{++}$, and $\boldsymbol{V}_{--}$ are full-rank for all $\eta \geq 0$. We discuss the meaning of this assumption and implications of its violation in Appendix B.

The exact parabolization of equation (7), in terms of $\boldsymbol{\psi}$, is

$$\frac{d\boldsymbol{\psi}_+}{dx} = \boldsymbol{D}_{++}\boldsymbol{\psi}_+, \tag{21a}$$

$$\boldsymbol{\psi}_- = \boldsymbol{0}. \tag{21b}$$

This can also be written in terms of the characteristic variables as

$$\frac{d\hat{\boldsymbol{\phi}}_+}{dx} = \boldsymbol{M}_{++}\hat{\boldsymbol{\phi}}_+ + \boldsymbol{M}_{+-}\hat{\boldsymbol{\phi}}_-, \tag{22a}$$

$$\boldsymbol{U}_{-+}\hat{\boldsymbol{\phi}}_+ + \boldsymbol{U}_{--}\hat{\boldsymbol{\phi}}_- = \boldsymbol{0}. \tag{22b}$$

Equation (22) is a differential–algebraic system of index 1, so $\hat{\boldsymbol{\phi}}_-$ can be eliminated, giving an ordinary differential equation for the positive characteristic variable:

$$\frac{d\hat{\boldsymbol{\phi}}_+}{dx} = \boldsymbol{M}_{++}^*\hat{\boldsymbol{\phi}}_+, \tag{23}$$

where

$$\boldsymbol{M}_{++}^* = \boldsymbol{M}_{++} - \boldsymbol{M}_{+-}\boldsymbol{U}_{--}^{-1}\boldsymbol{U}_{-+} \tag{24a}$$

$$= \begin{bmatrix} \boldsymbol{M}_{++} & \boldsymbol{M}_{+-} \end{bmatrix} \begin{bmatrix} \boldsymbol{I} \\ -\boldsymbol{U}_{--}^{-1}\boldsymbol{U}_{-+} \end{bmatrix} \tag{24b}$$

$$= \begin{bmatrix} \boldsymbol{V}_{++} & \boldsymbol{V}_{+-} \end{bmatrix} \begin{bmatrix} \boldsymbol{D}_{++} & \boldsymbol{0} \\ \boldsymbol{0} & \boldsymbol{D}_{--} \end{bmatrix} \begin{bmatrix} \boldsymbol{U}_{++} & \boldsymbol{U}_{+-} \\ \boldsymbol{U}_{-+} & \boldsymbol{U}_{--} \end{bmatrix} \begin{bmatrix} \boldsymbol{I} \\ -\boldsymbol{U}_{--}^{-1}\boldsymbol{U}_{-+} \end{bmatrix} \tag{24c}$$

$$= \begin{bmatrix} \boldsymbol{V}_{++} & \boldsymbol{V}_{+-} \end{bmatrix} \begin{bmatrix} \boldsymbol{D}_{++} & \boldsymbol{0} \\ \boldsymbol{0} & \boldsymbol{D}_{--} \end{bmatrix} \begin{bmatrix} \boldsymbol{V}_{++}^{-1} \\ \boldsymbol{0} \end{bmatrix} \tag{24d}$$

$$= \boldsymbol{V}_{++}\boldsymbol{D}_{++}\boldsymbol{V}_{++}^{-1}. \tag{24e}$$

In going from the third to fourth line, we made use of the identity $\boldsymbol{V}_{++}^{-1} = \boldsymbol{U}_{++} - \boldsymbol{U}_{+-}\boldsymbol{U}_{--}^{-1}\boldsymbol{U}_{-+}$. It is clear from the final equality that the eigenvalues of $\boldsymbol{M}_{++}^*$ are precisely the downstream eigenvalues of $\boldsymbol{M}$. The one-way equation is therefore well-posed and admits the proper rightgoing solutions.

Implementation of the exact one-way equation given by equation (22) would require calculation of the $N_-$ left eigenvectors corresponding to the leftgoing eigenvalues of $\boldsymbol{M}$. The resulting computational cost would usually be intolerably high. This is especially true for $x$-dependent systems, in which case local eigenvectors would need to be recalculated at each $x$ (see Section 2.4). Instead, we will generate a practical one-way equation by approximating the parabolization condition given by equation (22b).

## 2.3. Approximate one-way equation

Motivated by the connection between the exact one-way equation and nonreflecting boundary conditions, our approximate parabolization method is based on recursions that were introduced by Givoli and Neta [20] and Hagstrom and Warburton [21] for generating nonreflecting boundary conditions. Accordingly, we propose an approximate one-way equation given by the differential–algebraic system

$$\frac{d\hat{\boldsymbol{\phi}}_+}{dx} = \boldsymbol{M}_{++}\hat{\boldsymbol{\phi}}_+ + \boldsymbol{M}_{+-}\hat{\boldsymbol{\phi}}_-,$$                                    (25a)

$$\left(\boldsymbol{M} - i\beta_+^j \boldsymbol{I}\right)\hat{\boldsymbol{\phi}}^j = \left(\boldsymbol{M} - i\beta_-^j \boldsymbol{I}\right)\hat{\boldsymbol{\phi}}^{j+1} \qquad j = 0, \ldots, N_\beta - 1,$$                (25b)

$$\hat{\boldsymbol{\phi}}_-^{N_\beta} = 0.$$                                    (25c)

In this formulation, we have introduced a set of auxiliary variables $\{\hat{\boldsymbol{\phi}}^j : j = 0, \ldots, N_\beta\}$ and a set of complex scalar parameters $\{\beta_+^j, \beta_-^j : j = 0, \ldots, N_\beta - 1\}$. The zero-indexed variable is the physical variable ($\hat{\boldsymbol{\phi}}^0 = \hat{\boldsymbol{\phi}}$) and the remaining auxiliary variables are defined by the recursions. The selection of the recursion parameters will be discussed below. We call $N_\beta$ the order of the approximate one-way equation.

To verify that equation (25) is well-posed as a one-way equation, we examine its behavior in the limit as $\eta$ becomes large in accordance with Briggs' criterion. We stipulate that the recursion parameters remain bounded in this limit, which places no practical restriction on their values since they need only be defined at $\eta = 0$, and can be formally continued in any convenient manner for $\eta > 0$. Then, for sufficiently large $\eta$, equation (25b) is dominated by the terms involving $\boldsymbol{M}$, and we conclude that $\hat{\boldsymbol{\phi}}^j = \hat{\boldsymbol{\phi}}^{j+1}$ for all $j$. Then equation (25c) implies that $\hat{\boldsymbol{\phi}}_- = 0$, which when applied to equation (25a) eliminates the second term on the right-hand-side. For large $\eta$, $\boldsymbol{M}_{++}$ tends to the real, negative matrix $-\eta\tilde{\boldsymbol{A}}_{++}^{-1}$. All of the eigenvalues of this final matrix have $\alpha$ with positive imaginary part. Therefore, by construction, equation (25) admits only rightgoing modes and is well-posed as a one-way equation.

This represents a fundamental difference between the frequency domain one-way equations pursued in this paper and time domain one-way equations that are often used as nonreflecting boundary conditions. In the time domain case, any parameters that arise in the formulation must be specified as explicit functions of $s$ in order for the equations to be transformed back into the time domain. As a result, the choice of parameters critically effects the well-posedness of the approximate equations [4]. In contrast, the recursion parameters do not effect the well-posedness of our frequency domain one-way equations, allowing for great flexibility in the parameter selection process.

Next, we show that the approximate one-way equation converges to the exact one-way equation as the order of the approximation increases, provided that the recursion parameters are appropriately chosen. Since equation (25a) is identical to equation (22a), we must only show that equation (25b) and equation (25c) together converge to equation (22b). In other words, we wish to show that $\boldsymbol{\psi}_- \to 0$ as $N_\beta \to \infty$. To do so, we begin by defining $\boldsymbol{\psi}^j = \boldsymbol{U}\hat{\boldsymbol{\phi}}^j$, which is the natural extension of the previous definition $\boldsymbol{\psi} = \boldsymbol{U}\hat{\boldsymbol{\phi}}$. Equation (25b) can then be written

$$\left(\boldsymbol{D} - i\beta_+^j \boldsymbol{I}\right)\boldsymbol{\psi}^j = \left(\boldsymbol{D} - i\beta_-^j \boldsymbol{I}\right)\boldsymbol{\psi}^{j+1} \qquad j = 0, \ldots, N_\beta - 1.$$               (26)

Since $\boldsymbol{D}$ is diagonal, each scalar component of $\boldsymbol{\psi}^j$ can be considered separately:

$$\left(i\alpha_k - i\beta_+^j\right)\boldsymbol{\psi}_k^j = \left(i\alpha_k - i\beta_-^j\right)\boldsymbol{\psi}_k^{j+1} \qquad j = 0, \ldots, N_\beta - 1, \quad k = 1, \ldots, N.$$            (27)

It is then straightforward to eliminate all of the intermediate ($j = 1, .., N_\beta - 1$) auxiliary variables, leaving

$$\boldsymbol{\psi}_k^{N_\beta} = \mathcal{F}(\alpha_k)\boldsymbol{\psi}_k \qquad k = 1, \ldots, N$$                   (28)

with

$$\mathcal{F}(\alpha) = \prod_{j=0}^{N_\beta - 1} \frac{\alpha - \beta_+^j}{\alpha - \beta_-^j}.$$                              (29)

We now re-assemble equation (28) into a single matrix equation for all $k$:

$$\left\{ \begin{array}{c} \boldsymbol{\psi}_+^{N_\beta} \\ \boldsymbol{\psi}_-^{N_\beta} \end{array} \right\} = \left[ \begin{array}{cc} \boldsymbol{F}_{++} & \boldsymbol{0} \\ \boldsymbol{0} & \boldsymbol{F}_{--} \end{array} \right] \left\{ \begin{array}{c} \boldsymbol{\psi}_+ \\ \boldsymbol{\psi}_- \end{array} \right\},$$                        (30)

where $\boldsymbol{F}_{++}$ and $\boldsymbol{F}_{--}$ are diagonal matrices whose entries are the values of $\mathcal{F}(\alpha)$ associated with each rightgoing and leftgoing eigenvalue, respectively.

Next, we apply the termination condition given by equation (25c). To do so, we write the left-hand-side of equation (30) in terms of $\hat{\boldsymbol{\phi}}^{N_\beta}$:

$$\begin{bmatrix} \boldsymbol{U}_{++} & \boldsymbol{U}_{+-} \\ \boldsymbol{U}_{-+} & \boldsymbol{U}_{--} \end{bmatrix} \left\{ \begin{array}{c} \hat{\boldsymbol{\phi}}_+^{N_\beta} \\ \hat{\boldsymbol{\phi}}_-^{N_\beta} \end{array} \right\} = \begin{bmatrix} \boldsymbol{F}_{++} & \boldsymbol{0} \\ \boldsymbol{0} & \boldsymbol{F}_{--} \end{bmatrix} \left\{ \begin{array}{c} \boldsymbol{\psi}_+ \\ \boldsymbol{\psi}_- \end{array} \right\}. \tag{31}$$

Applying equation (25c) and eliminating $\hat{\boldsymbol{\phi}}_+^{N_\beta}$ leaves

$$\boldsymbol{\psi}_- = \boldsymbol{R}\boldsymbol{\psi}_+, \tag{32}$$

with

$$\boldsymbol{R} = \boldsymbol{F}_{--}^{-1}\boldsymbol{W}\boldsymbol{F}_{++}, \tag{33}$$

and

$$\boldsymbol{W} = \boldsymbol{U}_{-+}\boldsymbol{U}_{++}^{-1}. \tag{34}$$

The rectangular matrix $\boldsymbol{R}$ is analogous to a matrix of reflection coefficients. Each entry of $\boldsymbol{R}$ takes the form

$$\boldsymbol{r}_{mn} = \frac{\mathcal{F}(\alpha_{+,n})}{\mathcal{F}(\alpha_{-,m})}\boldsymbol{w}_{mn} \tag{35}$$

where $\alpha_{+,n}$ is the $n$th rightgoing eigenvalue, $\alpha_{-,m}$ is the $m$th leftgoing eigenvalue, and $\boldsymbol{w}_{mn}$ is the $(m, n)$ entry of the weighting matrix $\boldsymbol{W}$, which does not depend on the recursion parameters.

To achieve convergence to the exact one-way equation, every $\boldsymbol{r}_{mn}$ must converge toward zero as the order of the approximation increases. Since the weights are fixed, the recursion parameters must be chosen such that $\mathcal{F}(\alpha_{+,n})/\mathcal{F}(\alpha_{-,m})$ goes to zero for all $m$, $n$. This is accomplished by forcing $\mathcal{F}(\alpha_{+,n})$ to zero and $\mathcal{F}(\alpha_{-,m})$ to infinity.

The following geometric interpretation of $\mathcal{F}$ is helpful for choosing parameters that accomplish these objectives. Note that $\mathcal{F}$ is composed of a product of factors

$$\mathcal{F}^j(\alpha) = \frac{\alpha - \beta_+^j}{\alpha - \beta_-^j}. \tag{36}$$

It is clear that the magnitude of each individual factor is less than one for regions of the complex $\alpha$ plane that are closer to $\beta_+^j$ than $\beta_-^j$ ($|\alpha - \beta_+^j| < |\alpha - \beta_-^j|$) and greater than one for regions that are closer to $\beta_-^j$ than $\beta_+^j$ ($|\alpha - \beta_+^j| > |\alpha - \beta_-^j|$). Therefore, $\mathcal{F}(\alpha_{+,n})$ is driven to zero by placing the $\beta_+^j$ parameters near the rightgoing eigenvalues in the complex plane, and $\mathcal{F}(\alpha_{-,m})$ is driven to infinity by placing the $\beta_-^j$ parameters near the leftgoing eigenvalues.

Suppose that, for a given system, there exists a pair of parameters $\{\beta_+^0, \beta_-^0\}$ for which $|\mathcal{F}^0| < 1$ for all rightgoing eigenvalues and $|\mathcal{F}^0| > 1$ for all leftgoing eigenvalues. Furthermore, define $\kappa$ as the maximum value of $|\mathcal{F}^0(\alpha_{+,n})|/|\mathcal{F}^0(\alpha_{-,m})|$ over all $m$, $n$. If this parameter pair is then repeated for all $j = 0, \ldots, N_\beta - 1$, the slowest converging entry of $\boldsymbol{R}$ will decrease like $\kappa^{N_\beta}$ as the order of the approximation is increased. Therefore, even for this very simple choice of parameters, the method exhibits spectral convergence. In practice, it is not always possible to find a single pair of recursion parameters for which this supposition holds. Even if such a pair exists, it is typically preferable to distribute the parameters over a range of locations using the above distance-based guidelines, since eigenvalues close to a single repeated parameter converge much more rapidly than those farther away.

The question arises whether it is always possible to find a set of recursion parameters, for some sufficiently high $N_\beta$, that makes every $\boldsymbol{r}_{mn}$ arbitrarily small. Assuming that $\alpha_{+,n} \neq \alpha_{-,m}$ for all $m$, $n$, the answer is, surprisingly, yes. Specifically, the minimal set that accomplishes this is $\{\beta_+^n = \alpha_{+,n}, \ \beta_-^n \neq \alpha_{+,n} : n = 1, \ldots, N_+\}$ if $N_+ < N_-$ or $\{\beta_-^m = \alpha_{-,m}, \ \beta_+^m \neq \alpha_{-,m} : m = 1, \ldots, N_-\}$ if $N_- < N_+$. This of course requires complete knowledge of the eigenvalues of the discretized system, which is rarely possessed in practice. However, for systems that model physical phenomena, the locations of the rightgoing and leftgoing eigenvalues are physically meaningful and can often be estimated by studying simplified systems. This will be demonstrated for the Euler equations in 3.2. Furthermore, the spectra of discretized physical systems tend to be structured, such that groups of rightgoing eigenvalues often occupy different regions of the complex plane than groups of leftgoing eigenvalues. Again, this will often be the case for the Euler equations, even when linearized about nonuniform baseflows.

When eigenvalues cluster into groups, $\mathcal{F}$ can be driven to its desired limit for a large number of eigenvalues using a small number of parameters by taking advantage of the short distances between clustered eigenvalues and placing a parameter within the cluster. As will be shown in Section 2.5, it is precisely the fact that good approximations can be obtained for $N_\beta << N$ that makes the approximate one-way equations cost-effective.

## 2.4. Extension to x-dependent systems

In the previous two subsections, we developed exact and approximate one-way equations under the assumption that $\boldsymbol{M}$ is homogeneous in $x$. In this subsection, we discuss the extension of these methods to $x$-dependent systems.

First, it is easy to verify that for $x$-dependent systems, the approximate parabolization given by equation (25) still converges to the exact parabolization given by equation (22) at every $x$. Therefore, we must only evaluate the exact method, and all conclusions will apply also to the approximate formulation.

Central to the concept of parabolization is the identification of rightgoing and leftgoing parts of the solution at each axial location. When $\boldsymbol{M}$ is $x$-dependent, equation (7) no longer admits simple modal solutions, so Briggs' criterion no longer strictly applies. However, the theory of well-posedness of variable coefficient hyperbolic systems [19] provides a means by which to distinguish, locally at each $x$, parts of the solution that are rightgoing and leftgoing. Simply put, the variable coefficient extension of well-posedness theory states that constant coefficient analysis of the frozen coefficient system at a given $x$ provides the correct (that is, well-posed) division of the solution into rightgoing and leftgoing components. Therefore, the one-way equations derived in the previous two sections will still retain and eliminate the correct parts of the operator at each axial station for $x$-dependent systems, and the equations therefore remain well-posed.

The fundamental difference between the homogeneous and $x$-dependent cases is that in the later, the rightgoing and leftgoing variables no longer evolve *independently*. Except in rare cases, the eigen-expansion $\hat{\boldsymbol{\phi}} = \boldsymbol{V}\boldsymbol{\psi}$ no longer diagonalizes equation (7) because $\frac{d\boldsymbol{V}}{dx} \neq \boldsymbol{0}$. As a result, every expansion coefficient $\boldsymbol{\psi}_k$ is potentially coupled with every other coefficient. This coupling is intrinsic to $x$-dependent equations and is deeply linked to important properties of their solutions. For example, this coupling allows convective solution of the linearized Euler equations to excite acoustic waves that propagate in all directions.

The implication of this coupling for our one-way equation is that setting $\boldsymbol{\psi}_- = \boldsymbol{0}$ will cause $\boldsymbol{\psi}_+$ to evolve incorrectly as it propagates. Therefore, accurate one-way approximations can only be obtained when leftgoing waves have a *weak* influence on the evolution of the rightgoing waves. This is not a shortcoming of our particular parabolization method, but rather an inherent limitation on the class of problems for which a one-way solution strategy is sensible. An important situation in which the coupling is weak occurs when the system is *slowly-varying* in $x$. In this case, the slow variation of the system ensures the slow variation of $\boldsymbol{V}$, which in turn implies that the eigen-expansion nearly diagonalizes $\boldsymbol{M}$. A close examination of the meaning of "nearly diagonalizes" reveals that this is akin to the usual short-wavelength condition that is frequently invoked when extending local theory to spatially-varying equations.

To reiterate, the one-way equations are well-posed for all hyperbolic systems, but physical accuracy is guaranteed only for those that are sufficiently slowly-varying in $x$.

## 2.5. Computational cost

As mentioned in the introduction, the value of one-way approximations is their low computational cost compared to traditional solution techniques. We now compare operation count scaling estimates for several methods.

Using the approximate one-way equations entails satisfying the differential–algebraic system given by equation (25) at each axial step in the march. This, in turn, requires the solution of a matrix system with leading dimension $\mathcal{O}(N_y N_\beta)$. For efficiency, it is important for the system to be sparse, which, in turn, requires the use of sparse discretization schemes. When this requirement is observed, the banded structure of the system results in a predicted operation count that scales like $N_y N_\beta^2$. Modern sparse solvers can often exploit additional structure within the system not accounted for in this simple cost estimate, and in practice we observe scaling like $N_y N_\beta^p$ with $1 < p < 2$. Frequently, $p \approx 1.5$.

The eigen-solution required by the exact parabolization method scales like $N_y^3$. The cost savings of the approximate method stems from the fact that $N_\beta \ll N_y$ and therefore $N_\beta^p \ll N_y^2$. Because of the impracticality of the exact parabolization method, from here on out we will refer to the approximate formulation as *the* one-way equations. Direct time domain and frequency domain solutions of the original hyperbolic system scale like $N_y N_t$ and $N_y^2$, respectively, per axial station. In time domain solvers, $N_t$ is the number of time steps required to obtain a stationary solution. Again, the benefit of the one-way equations is that $N_\beta^p \ll N_t$. Finally, PSE usually scales like $N_y N_{it}$, where $N_{it}$ is the number of iterations required to satisfy a nonlinear constraint that is part of the PSE formulation. PSE is typically cheaper than the one-way equations since in most cases $N_{it} < N_\beta^p$.

## 3. Application to the Euler equations

In this section, our one-way methodology is applied to the linearized Euler equations. The primary task is to determine robust recursion parameters that can be used for a range of problems. To achieve this, we first use analytical eigenvalues for a uniform flow to predict the approximate locations of the eigenvalues of the semi-discretized equations for nonuniform flows. Using these estimates, strategies developed by Hagstrom and colleagues [21–24] for choosing parameters for nonreflecting boundary conditions can be adapted to select recursion parameters that result in accurate and convergent one-way equations for many flows. The development outlined here for the Euler equations can be used as a guide for identifying appropriate recursion parameters when applying the method to other hyperbolic systems of equations.

### 3.1. Linearized Euler equations

The linearized Euler equations in three-dimensional Cartesian coordinates can be written in the form of equation (1) with $d = 3$,

$$
A = \begin{bmatrix} \bar{u}_x & -\bar{v} & 0 & 0 & 0 \\ 0 & \bar{u}_x & 0 & 0 & \bar{v} \\ 0 & 0 & \bar{u}_x & 0 & 0 \\ 0 & 0 & 0 & \bar{u}_x & 0 \\ 0 & \gamma\bar{p} & 0 & 0 & \bar{u}_x \end{bmatrix}, \qquad
B_1 = \begin{bmatrix} \bar{u}_{y_1} & 0 & -\bar{v} & 0 & 0 \\ 0 & \bar{u}_{y_1} & 0 & 0 & 0 \\ 0 & 0 & \bar{u}_{y_1} & 0 & \bar{v} \\ 0 & 0 & 0 & \bar{u}_{y_1} & 0 \\ 0 & 0 & \gamma\bar{p} & 0 & \bar{u}_{y_1} \end{bmatrix},
$$

$$
B_2 = \begin{bmatrix} \bar{u}_{y_2} & 0 & 0 & -\bar{v} & 0 \\ 0 & \bar{u}_{y_2} & 0 & 0 & 0 \\ 0 & 0 & \bar{u}_{y_2} & 0 & 0 \\ 0 & 0 & 0 & \bar{u}_{y_2} & \bar{v} \\ 0 & 0 & 0 & \gamma\bar{p} & \bar{u}_{y_2} \end{bmatrix}, \qquad
C = \begin{bmatrix} -\nabla\cdot\bar{u} & \frac{\partial\bar{v}}{\partial x} & \frac{\partial\bar{v}}{\partial y_1} & \frac{\partial\bar{v}}{\partial y_2} & 0 \\ \frac{\partial\bar{p}}{\partial x} & \frac{\partial\bar{u}_x}{\partial x} & \frac{\partial\bar{u}_x}{\partial y_1} & \frac{\partial\bar{u}_x}{\partial y_2} & 0 \\ \frac{\partial\bar{p}}{\partial y_1} & \frac{\partial\bar{u}_{y_1}}{\partial x} & \frac{\partial\bar{u}_{y_1}}{\partial y_1} & \frac{\partial\bar{u}_{y_1}}{\partial y_2} & 0 \\ \frac{\partial\bar{p}}{\partial y_2} & \frac{\partial\bar{u}_{y_2}}{\partial x} & \frac{\partial\bar{u}_{y_2}}{\partial y_1} & \frac{\partial\bar{u}_{y_2}}{\partial y_2} & 0 \\ 0 & \frac{\partial\bar{p}}{\partial x} & \frac{\partial\bar{p}}{\partial y_1} & \frac{\partial\bar{p}}{\partial y_2} & \gamma\nabla\cdot\bar{u} \end{bmatrix},
$$

and $q = \{v, u_x, u_{y_1}, u_{y_2}, p\}^T$. We have chosen as independent variables specific volume $v$, velocity $u = \{u_x, u_{y_1}, u_{y_2}\}^T$, and pressure $p$. The equations are linearized about a baseflow $\bar{q} = \{\bar{v}, \bar{u}_x, \bar{u}_{y_1}, \bar{u}_{y_2}, \bar{p}\}^T$, and all variables have been appropriately non-dimensionalized by an ambient sound speed and density and a problem dependent length-scale. The fluid is approximated as a perfect gas with specific heat ratio $\gamma$.

The eigenvalues and diagonalizing transformation of $A$ are

$$
\tilde{A} = \begin{bmatrix} \bar{u}_x & 0 & 0 & 0 & 0 \\ 0 & \bar{u}_x & 0 & 0 & 0 \\ 0 & 0 & \bar{u}_x & 0 & 0 \\ 0 & 0 & 0 & \bar{u}_x+\bar{c} & 0 \\ 0 & 0 & 0 & 0 & \bar{u}_x-\bar{c} \end{bmatrix}, \qquad
T = \begin{bmatrix} 1 & 0 & 0 & 0 & (\bar{v}/\bar{c})^2 \\ 0 & 0 & 1 & 0 & 0 \\ 0 & 0 & 0 & 1 & 0 \\ 0 & 1 & 0 & 0 & \bar{v}/\bar{c} \\ 0 & 1 & 0 & 0 & -\bar{v}/\bar{c} \end{bmatrix},
$$

where $\bar{c} = (\gamma\bar{p}\bar{v})^{1/2}$ is the speed of sound. The semi-discretized operators $\tilde{\boldsymbol{A}}$ and $\boldsymbol{T}$ are found by sampling $\tilde{A}$ and $T$, respectively, at the discretization points.

### 3.2. Parameter selection

The critical step in applying our one-way methodology to any system of equations is determining appropriate recursion parameters. As discussed in Section 2.3, this requires knowledge of the eigenvalues of the semi-discretized operator $\boldsymbol{M}$ – specifically their location in the complex plane and their direction (rightgoing or leftgoing). For many baseflows, the eigenvalues of the semi-discretized equations form predictable groups that can be approximated and classified using the eigenvalues supported by a uniform flow. These uniform flow eigenvalues can be computed analytically, and therefore provide a means by which to predict the locations and directions of the eigenvalues for nonuniform baseflows. These estimates, in turn, can be used to define recursion parameters that result in convergent one-way approximations of the nonuniform equations.

We now derive the spatial eigenvalues of the Euler equations linearized about a uniform flow. For a uniform baseflow, $C = 0$ and the entries of the remaining three matrix coefficients are constants. Because of this, the transverse directions can be Fourier transformed rather than discretized. Then equation (1) reduces to

$$
\frac{\partial q^\dagger}{\partial t} + A\frac{\partial q^\dagger}{\partial x} + ik_1 B_1 q^\dagger + ik_2 B_2 q^\dagger = 0, \tag{38}
$$

where $q^\dagger$ is the Fourier transform of $q$ and $k_{1,2}$ are the Fourier duals of $y_{1,2}$. Proceeding as in Section 2.1, equation (38) is then written in terms of its characteristic variables $\phi^\dagger = Tq^\dagger$, Laplace transformed in time, and solved for the axial derivative term, finally resulting in an equation of the form

$$
\frac{d\hat{\phi}^\dagger}{dx} = M^\dagger \hat{\phi}^\dagger \tag{39}
$$

with

$$
M^\dagger = ikTA^{-1}(I - z_1 B_1 - z_2 B_2)T^{-1}. \tag{40}
$$

**Table 1**
Classification of the eigenvalues of the uniform Euler equations: rightgoing (+), leftgoing (−), or singular (0).

| Eigenvalue | $\bar{M}_x < -1$ | $\bar{M}_x = -1$ | $-1 < \bar{M}_x < 0$ | $\bar{M}_x = 0$ | $0 < \bar{M}_x < 1$ | $\bar{M}_x = 1$ | $\bar{M}_x > 1$ |
|---|---|---|---|---|---|---|---|
| $\alpha_c$ | − | − | − | 0 | + | + | + |
| $\alpha_{a_1}$ | − | 0 | + | + | + | + | + |
| $\alpha_{a_2}$ | − | − | − | − | − | 0 | + |

Here, $\hat{\phi}^\dagger$ is the Laplace transform of $\phi^\dagger$, $k = (\omega + i\eta)/\bar{c}$ is a scaled Laplace variable, and $z_{1,2} = k_{1,2}/k$ are scaled transverse wavenumbers.

The eigenvalues of $M$ are

$$i\alpha_c = \frac{ik}{\bar{M}_x}, \qquad i\alpha_{a_1}(z) = ik\frac{-\bar{M}_x + \mu(z)}{1 - \bar{M}_x^2}, \qquad i\alpha_{a_2}(z) = ik\frac{-\bar{M}_x - \mu(z)}{1 - \bar{M}_x^2}, \qquad (41)$$

where $\bar{M}_x = \bar{u}_x/\bar{c}$ is the local Mach number, $z = \left(z_1^2 + z_2^2\right)^{1/2}$ is a composite wavenumber, and the function $\mu(z)$ is given by

$$\mu(z) = \sqrt{1 - (1 - \bar{M}_x^2)z^2}. \qquad (42)$$

The discrete eigenvalue $i\alpha_c$ has multiplicity three and describes the convection of entropy and vorticity, while the remaining two eigenvalues are continuous branches and describe both propagating and evanescent acoustic waves.

Each of these eigenvalues can be identified as either rightgoing or leftgoing for different values of the Mach number using Briggs' criterion. Each eigenvalue also has a singular point at a particular Mach number corresponding to a singular point of $A$. This is discussed further in Appendix B, but for the purpose of parameter selection these infinite eigenvalues can be ignored. The results are summarized as a function of the Mach number in Table 1, in which a (+) indicates that an eigenvalue is rightgoing, a (−) indicates that an eigenvalue is leftgoing, and a zero indicates a singular point. With these directions determined, we set $\eta = 0$ from here on out.

The eigenvalues of semi-discretized nonuniform Euler equations can often be sorted into groups associated with these three uniform flow eigenvalues. First, nonuniform Euler equations typically support convective modes that travel with phase speeds ranging from the slowest to fastest axial velocities within the flow. The location and direction of these eigenvalues are given by evaluating $\alpha_c$ with $\bar{M}_x$ varied over this range of velocities.

Second, nonuniform Euler equations usually support branches of acoustic modes that are well approximated by $\alpha_{a_1}$ and $\alpha_{a_2}$ with $\bar{M}_x$ set to its asymptotic value as $|y|$ becomes large. If multiple asymptotic values of $\bar{M}_x$ exist, multiple branches of acoustic eigenvalues will exist that can be approximated by evaluating $\alpha_{a_1}$ and $\alpha_{a_2}$ separately at each asymptotic value. These uniform flow acoustic eigenvalues are continuous branches while the eigenvalues of the semi-discretized nonuniform equations are necessarily discrete. One consequence of this is that the continuous eigenvalues need only be considered up to the maximum wavenumber $z_{max}$ that is supported by the transverse grid, since no eigenvalues of the semi-discretized equations exist beyond this limit.

These eigenvalue estimates can also be used when the Euler equations are written in different coordinate systems. The uniform flow equations in two-dimensional Cartesian coordinates admit the same analytical eigenvalues, but the convective eigenvalue has multiplicity two instead of three. When written in cylindrical coordinates, some of the matrix coefficients depend on the radial coordinate, so strictly speaking, analytical eigenvalues cannot be derived using spatial Fourier transforms. In spite of this, we have found that the above eigenvalues still provide a good representation of the discretized eigenvalues for both uniform and nonuniform baseflows.

These predictions for the locations and directions of the eigenvalues of $\boldsymbol{M}$ can now be used to choose appropriate recursion parameters. As established in Section 2.3, the $\beta_+^j$ parameters must be placed near the rightgoing eigenvalues so that $\mathcal{F}$ is small for every rightgoing eigenvalue, while the $\beta_-^j$ parameters must be placed near the leftgoing eigenvalues so that $\mathcal{F}$ is large for every leftgoing eigenvalue. In other words, the $\beta_+^j$ and $\beta_-^j$ parameters should be distributed over the predicted locations of the rightgoing and leftgoing eigenvalues, respectively.

As an example, we expound this procedure for the commonly encountered case where $0 < \bar{M}_x < 1$ everywhere in the flow. Then $\alpha_c$ and $\alpha_{a_1}$ are rightgoing while $\alpha_{a_2}$ is leftgoing. A complete set of recursion parameters is constructed by defining several subsets related to different parts of the predicted spectrum. Strategies for choosing these subsets are described in the following paragraphs, and their precise definitions are given in Table 2.

First, a set $\beta_\pm^c$ with $N_c$ parameter pairs is defined with the goal of making $\mathcal{F}$ small for the convective eigenvalues. The $\beta_+^j$ parameters are evenly distributed over the range of predicted values of $\alpha_c$. The corresponding $\beta_-^j$ parameters should be placed far away from the convective eigenvalues so that the magnitude of the $\mathcal{F}^j$ factors for these parameters are as small as possible in the vicinity of the convective eigenvalues. However, it is also desirable for these $\mathcal{F}^j$ factors to be small at $\alpha_{a_1}$ and large at $\alpha_{a_2}$. A good compromise between these two competing objectives is obtained by rotating the $\beta_+^c$ parameters by $-90$ degrees around the asymptotic value of $\bar{M}_x$ that is used to predict the acoustic parameters. Then, $|\mathcal{F}^j| \leq 1$ for all values of $\alpha_{a_1}$ and $|\mathcal{F}^j| \geq 1$ for all values of $\alpha_{a_2}$.

**Table 2**
Recursion parameter sets that target the three predicted groups of eigenvalues for $0 < \bar{M}_x < 1$.

| Type | Spacing | $\beta_+^j/k$ | $\beta_-^j/k$ |
|---|---|---|---|
| **Convective** | $b^h = \frac{1}{M_{max}} + \left(\frac{1}{M_{min}} - \frac{1}{M_{max}}\right)\frac{h}{N_c - 1}$ | $b^j$ | $-ib^j + (1+i)\frac{-\bar{M}_x}{1 - \bar{M}_x^2}$ |
| $\beta_\pm^c = \{\beta_\pm^j : j = 0, \ldots, N_c - 1\}$ | $h = 0, \ldots, N_c - 1$ | | |
| **Acoustic, propagating** | $\theta^h = \frac{\pi}{2}\frac{h}{2N_p}$ | $\dfrac{-\bar{M}_x + \cos\theta^{2j}}{1 - \bar{M}_x^2}$ | $\dfrac{-\bar{M}_x - \cos\theta^{2j+1}}{1 - \bar{M}_x^2}$ |
| $\beta_\pm^p = \{\beta_\pm^j : j = 0, \ldots, N_p - 1\}$ | $h = 0, \ldots, 2N_p - 1$ | | |
| **Acoustic, evanescent** | $\mu^h = \mu_{max}\frac{h}{2N_e}$ | $\dfrac{-\bar{M}_x + \mu^{2j}}{1 - \bar{M}_x^2}$ | $\dfrac{-\bar{M}_x - \mu^{2j+1}}{1 - \bar{M}_x^2}$ |
| $\beta_\pm^e = \{\beta_\pm^j : j = 0, \ldots, N_e - 1\}$ | $h = 0, \ldots, 2N_e - 1$ | | |

In choosing parameters to target the predicted acoustic eigenvalues, we exploit the rotational symmetry between $\alpha_{a_1}$ and $\alpha_{a_2}$ (about $k\frac{-\bar{M}_x}{1-\bar{M}_x^2}$ for each asymptotic value of $\bar{M}_x$). This allows parameter pairs to be chosen that simultaneously make the corresponding $\mathcal{F}^j$ factors small for the rightgoing eigenvalues and large for the leftgoing eigenvalues. Specifically, the $\beta_+^j$ parameters are distributed along $\alpha_{a_1}$ and the $\beta_-^j$ parameters are distributed along $\alpha_{a_2}$. The most straightforward approach to distributing the parameters is to choose a set of values of $z$ or $\mu(z)$ and define the pairs by evaluating both acoustic eigenvalues at each value. This choice guarantees the desired behavior of the $\mathcal{F}^j$ factors. However, Hagstrom et al. [24] showed that the uniform flow reflection coefficient (which is the analytical analogous to equation (32)) can be made zero at twice as many locations by offsetting the points at which $\alpha_{a_1}$ and $\alpha_{a_2}$ are evaluated.

Note that $\alpha_{a_1}$ and $\alpha_{a_2}$ are purely real up to a critical value of $z$, at which point they become purely imaginary. The real parts of the branches correspond to propagating acoustic waves, while the imaginary parts represent evanescent acoustic waves. We distribute the parameter pairs separately for these two sections of the branches. For the propagating modes, the angle of propagation is $\theta = \cos^{-1}(\mu(z))$. To choose a set $\beta_\pm^p$ with $N_p$ offset parameter pairs, take $2N_p + 1$ equally spaced angles on the closed interval $[0, \pi/2]$ and discard the final angle $\theta = \pi/2$. Then, starting with $\theta = 0$, use every-other angle to define a $\beta_+^j$ and $\beta_-^j$ parameter. To choose a set $\beta_\pm^e$ with $N_e$ parameters for the evanescent section of the acoustic branches, define $2N_e + 1$ equally spaced points on the closed interval $[0, \mu(z_{max})]$ and discard the point $\mu = 0$. Then, starting with the next value, use every-other point to define a $\beta_+^j$ and $\beta_-^j$ parameter.

The reason for omitting the values $\theta = \pi/2$ and $\mu(z) = 0$ (which are the same point in the complex plane) in both acoustic parameter sets is that they represent energy transfer that is tangent to the parabolization axis, which can never be captured by one-way spatial marching. Furthermore, the rightgoing branch $\alpha_{a_1}$ and the leftgoing branch $\alpha_{a_2}$ intersect at this point, and it is clearly impossible to make $\mathcal{F}$ both large and small at the same time. This is of no practical concern because the equivalent branches that occur in discretized equations do not intersect in this manner due to the incorporation of nonreflecting transverse boundary conditions (see for example the eigenvalues in Fig. 2).

Rather than defining the acoustic parameters using equally spaced angles (propagating) and points along $\mu$ (evanescent), the parameters can instead be chosen by formally minimizing $\mathcal{F}(\alpha_{a_1})/\mathcal{F}(\alpha_{a_2})$ with respect to some norm. Following Hagstrom and Warburton [22], we have carried out this calculation using a weighted minimax norm, but found very little improvement over equal spacing. The optimized parameters offered moderate improvements at high propagation angles, but at the cost of a degradation of evanescent and low angles waves. In practice, we therefore use the simple approach based on equal spacing.

The final set of recursion parameters is defined by taking the union of all of the subsets related to the different parts of the predicted spectrum. Typically, we use roughly the same number of parameters for each subset.

## 4. Results

In this section, we use the one-way Euler equations to solve three problems. First, a simple case involving the propagation of monopole acoustic waves in a quiescent fluid is used to demonstrate the convergence of the one-way equations. Second, the scattering of acoustic waves by a vortex is calculated using the one-way equations and compared to published direct-numerical-simulation results. Third, convectively unstable models of a compressible jet are solved using the one-way equations and compared to traditional time domain and PSE solutions of the same equations.

For all simulations, the equations are discretized in the transverse direction using fourth-order central finite differences with summation-by-parts boundary closure [25]. Far-field radiation boundary conditions are enforced at free transverse boundaries using a super-grid damping layer [26] truncated by Thompson characteristic conditions [27]. For the cylindrical coordinates calculations, pole conditions are implemented using the scheme of Mohseni and Colonius [28]. The one-way Euler equations are integrated in $x$ using a third-order, L-stable diagonally-implicit Runge–Kutta scheme [29]. Recursion parameters are selected using the strategies described in the previous section.
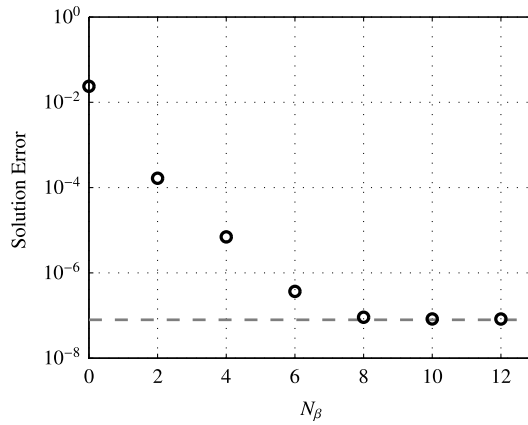
**Fig. 1.** Solution error (defined in equation (43)) for the monopole problem for the approximate (○) and exact (— — —) one-way Euler equations.

### 4.1. Monopole acoustic waves in a quiescent fluid

In this problem, a monopole disturbance is placed just upstream of the computational domain in a quiescent fluid. The monopole generates an acoustic field for which an analytical solution exists. Since the system is *x*-independent and the solution is comprised exclusively of downstream propagating waves, this set-up allows the convergence of the one-way equation to be verified.

The computational domain extends six wavelengths in both *x* and *y* and is discretized using 300 equally spaced points in each direction. Along the inlet of the domain, the exact monopole solution is supplied as an incoming fluctuation which is then propagated through the domain by integrating the one-way Euler equations. The calculation is performed using different orders of the approximation and also using the exact one-way equation. The solution error is defined as

$$\frac{1}{\mathcal{A}} \int_{\mathcal{A}} \left| \frac{p_{owe} - p_{exact}}{p_{max}} \right|^2 d\mathcal{A}, \tag{43}$$

where $p_{owe}$ is the pressure computed by the one-way Euler equations, $p_{exact}$ is the exact analytical pressure, and $p_{max}$ is the maximum value of the exact pressure in the domain. The integration is over the area $\mathcal{A}$ of the physical domain, not including the far-field damping layers.

The solution error results are plotted in Fig. 1. The convergence of the one-way solution over $0 < N_\beta < 8$ is spectral. For $N_\beta > 8$, the error plateaus at a level equal to the error of the exact one-way solution. Recall that the one-way Euler eigenvalues converge toward the eigenvalues of the *discretized* equations; the properties of the underlying discretization are unaltered by the parabolization method. Therefore, the convergence plateau indicates that the parabolization error has become smaller than other numerical errors, such as those related to boundary conditions and finite difference approximation. By the time this occurs for the discretization used here, the error in the one-way solution has dropped by five orders of magnitude.

A useful way to visualize the convergence of the method is to compare the eigenvalues of the one-way operator to those of the full operator *M*. As the one-way system converges, its eigenvalues should converge to the rightgoing eigenvalues of *M*. For the problem under consideration, all of the eigenvalues of *M* correspond to either rightgoing or leftgoing acoustic waves; no convective eigenvalues exist because the fluid is quiescent.

Fig. 2 compares the eigenvalues at several orders of the approximation. At $N_\beta = 0$, the upstream acoustic waves have been removed (since the equations are well-posed even at zero order), but the downstream eigenvalues are poorly represented. As $N_\beta$ is increased, all the eigenvalues of the one-way system converge toward the rightgoing eigenvalues of the full operator. The convergence is quantified in Fig. 3 for four eigenvalues corresponding to acoustic radiation to approximately 20, 40, 60 and 80 degrees to the parabolization axis (based on a simple plane-wave estimate). As expected, the higher angle eigenvalue converges more slowly than the lower angle eigenvalues, but the steady spectral convergence for all four angles confirms the quality of the recursion parameters that were derived in the previous section. The specific values of $\beta_+^j$ and $\beta_-^j$ used are also shown graphically in Fig. 2.

### 4.2. Scattering of acoustic waves by a vortex

Here, we use the one-way Euler equations to calculate the scattering of a plane acoustic wave by a homentropic vortex. This problem was previously investigated using a one-way wave equation [30] (which the author called a parabolic approximation) and direct numerical simulation [31]. We will compare our one-way Euler results to the later.
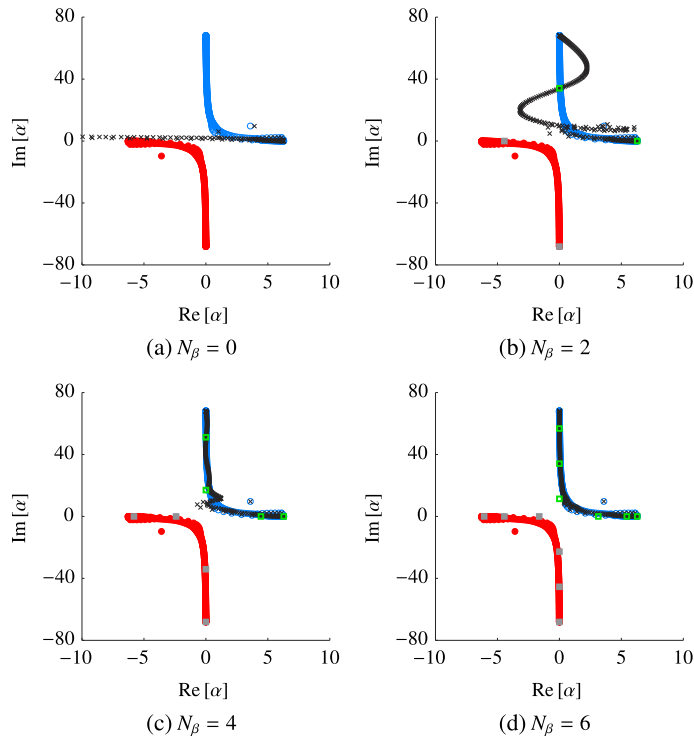
**Fig. 2.** Comparison between the eigenvalues of the full and one-way Euler operators for the monopole problem at several orders of the approximation. The full equations support rightgoing ($\bigcirc$) and leftgoing ($\bullet$) acoustic modes. The eigenvalues of the one-way equations ($\times$) converge to the rightgoing modes. Also shown are the $\beta_+^j$ ($\square$) and $\beta_-^j$ ($\blacksquare$) recursion parameters used for each order of the approximation.
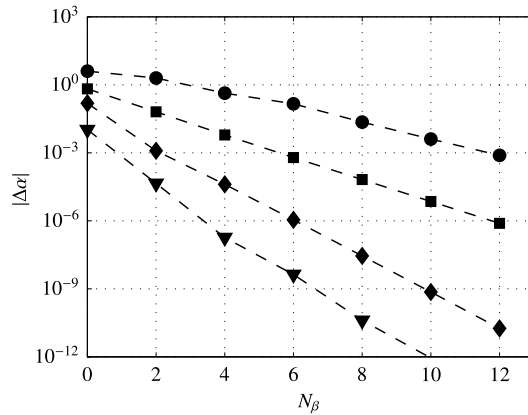


**Fig. 3.** Distance between the exact and one-way Euler eigenvalue for the monopole problem corresponding to acoustic radiation to several angles relative to the axis of parabolization: 20° ($\blacktriangledown$); 40° ($\blacklozenge$); 60° ($\blacksquare$); 80° ($\bullet$).

In our formulation, the Euler equations are linearized about a steady, homentropic vortex that exactly satisfies the two-dimensional nonlinear Euler equations. The tangential velocity about the center of the vortex is

$$\bar{u}_\theta = \frac{\Gamma}{2\pi r} \left( 1 - \exp\left(-ar^2\right) \right) \tag{44}$$

where $a = 1.256431$ is a constant chosen such that the maximum velocity occurs at $r = 1$. We define this to be the core radius, and nondimensionalize by this length scale. The radial velocity is zero and the pressure is given by

$$\bar{p} = \frac{1}{\gamma} \left( 1 - \frac{(\gamma - 1)\Gamma^2}{4\pi^2 r^2} f\left(ar^2\right) \right)^{\frac{\gamma}{\gamma - 1}} \tag{45}$$
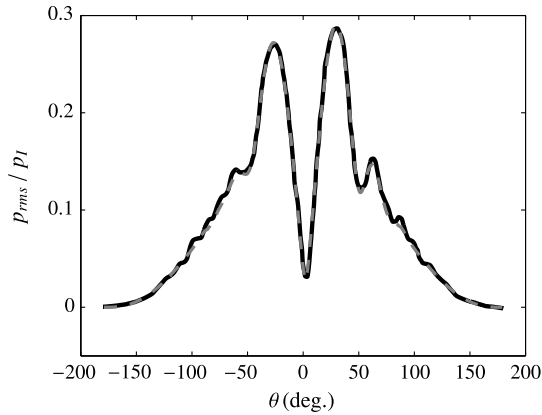
where

**Fig. 4.** Root-mean-square pressure level of the scattered wave at $r = 10$ computed by: direct numerical simulation (———) and the one-way Euler equations (— — —).

$$f(w) = \frac{1}{2} - \exp(-w) + \frac{1}{2}\exp(-2w) + w\,\mathrm{Ei}(-2w) - w\,\mathrm{Ei}(-w) \tag{46}$$

and Ei is the exponential integral function. The specific volume is related to the pressure by the homentropic relation

$$\bar{v} = (\gamma\bar{p})^{\frac{-1}{\gamma}}. \tag{47}$$

The maximum mean velocity induced by the vortex is

$$\bar{u}_\Gamma = \frac{\Gamma}{2\pi}. \tag{48}$$

We set $\bar{u}_\Gamma = 0.0625$ to match one of the DNS cases [31].

The computational domain extends ten core radii in $x$ and $y$ from the center of the vortex, and the transverse $y$ direction is discretized using 250 equally spaced points. An incoming plane acoustic wave with a wavelength of four core radii is specified at the left-hand boundary, and advanced by integrating the one-way equations with a step size of $\Delta x = 0.08$, corresponding to 50 points per wavelength. The solution is well converged using $N_\beta = 12$.

The scattered wave field is defined as the difference between the wave distorted by the vortex and an undistorted plane wave. In Fig. 4, the root-mean-square of the scattered pressure at $r = 10$ is plotted as a function of angle, with $\theta = 0°$ corresponding to the forward direction of the incident wave. The DNS results of Colonius et al. [31] are also shown. The agreement between the two solutions is excellent. The discernible error is confined to high forward angles ($80° < \theta < 90°$) and backward angles ($\theta > 90°$) for which the one-way solution is expected to degrade. The reasonable accuracy even at these high angles reveals that the scattered wave field at these angles is dominated by refraction effects due to the slowly decaying vortex rather than direct scattering from the vortex core, since by definition the one-way solution does not contain leftgoing waves.

Analogous results can be obtained for stronger vortices up to $\bar{u}_\Gamma = 0.2$. Above this threshold, spurious eigenvalues appear in the spectrum of **M** that are not properly accounted for using our standard set of recursion parameters, leading to insta-bility of the march. This highlights a limitation of our one-way methodology: recursion parameters must be specified that properly converge all of the eigenvalues of the discretized system, including those associated with both spurious nonphysical and unexpected physical dynamics. In this case, the offending eigenvalues are spurious – that is, a nonphysical artifact of the discretization. Such eigenvalues are by definition sensitive to details of the discretization, making them difficult to account for in the parameter selection process. It is likely that more sophisticated approaches to selecting parameters could alleviate this issue, but it's also worth emphasizing that our simple approach has proven effective for the majority of problems so far encountered.

### 4.3. Linear wavepackets in a Mach 0.9 turbulent jet

Finally, we use the one-way equations to compute linear wavepackets and their associated acoustic radiation in a Mach 0.9 jet. Wavepacket-based jet noise models have recently received a great deal of attention due to their ability to capture many important features of both the near-field jet turbulence and the resulting far-field acoustics (see the recent review by Jordan and Colonius [32]). This problem also exemplifies the typical properties of convectively unstable flows. The near-field mixing region is dominated by a single convective mode associated with the Kelvin–Helmholtz instability. The spatial growth and subsequent decay of this mode forms a wavepacket and causes the emission of acoustic waves that are very weak compared to the near-field fluctuations. This amplitude difference makes the acoustic radiation difficult to properly capture using approximate solution techniques and makes this a challenging test for our one-way equations.
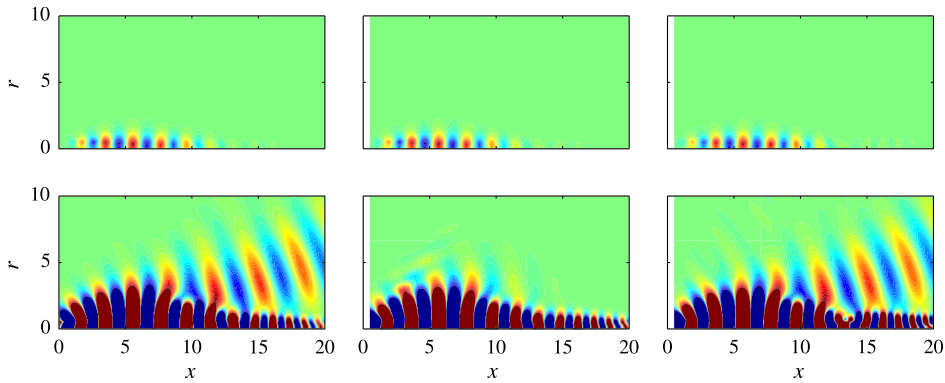
**Fig. 5.** Contours of axisymmetric pressure fluctuations at $St = 0.35$ in a Mach 0.9 jet, scaled by the maximum amplitude. Top row: fifty equally spaced contour levels between $\pm 1$. Bottom row: fifty equally spaced contour levels between $\pm 4 \times 10^{-3}$, chosen to show acoustic radiation. First column: direct solution. Second column: PSE. Third column: one-way Euler equations. The one-way Euler solution captures both the near-field wavepacket and the associated acoustic radiation at a fraction of the cost of the direct solution, while PSE completely misses the acoustic radiation.

In the specific problem considered here, the Navier–Stokes equations are linearized about the mean turbulent flow-field from a carefully validated large-eddy-simulation of an isothermal Mach 0.9 jet [33,34]. Axial second derivatives are neglected, as they are in other spatial marching methods such as the reduced and parabolized Navier–Stokes equations [17]. Radial and azimuthal second derivatives are retained. As discussed in 2.1, this ruins the hyperbolicity of the continuous system, but has no bearing on the parabolization process since the semi-discrete system defined in equation (2) remains hyperbolic. The computational domain extends fifteen jet diameters in the radial direction, and is discretized with 600 points that are clustered near the jet lip line ($r = 1/2$).

Half a diameter downstream of the inlet, the local Kelvin–Helmholtz eigenfunction is specified as an incoming fluctuation. The system is solved using the one-way Euler equations with $N_\beta = 12$, and also using the parabolized stability equations, which have frequently been employed within the context of wavepacket-based jet noise modeling [35,36]. We also compare to a previous solution [37] computed using time-domain integration, which we call the direct solution. Since this solution captures radiation is all directions, it can be thought of as the correct solution of the linear system.

Fig. 5 shows the axisymmetric part of the pressure fluctuation at a Strouhal number of $St = \frac{fD}{U_{jet}} = 0.35$, which is near the most amplified frequency. The direct, PSE, and one-way Euler solutions appear in the first, second, and third column, respectively. In the top row, contour levels are chosen to show the near-field wavepacket, which is approximated well by both the PSE and one-way Euler solutions. In the bottom row, the contour levels are reduced to highlight the acoustic radiation, which is almost three orders of magnitude smaller than the near-field fluctuations. The direct solution contains a beam of acoustic radiation that propagates to the far-field. Unlike the PSE solution, the one-way Euler solution accurately captures this acoustic radiation. The advantage of the one-way solution over the direct solution is computational speed: the direct solution used 37.5 CPU hours while the one-way solution used only 1.2 CPU hours, a 34 times speed-up. For comparison, the PSE solution required 0.063 CPU hours, but this speed is achieved at the expense of accuracy.

## 5. Conclusions

In this paper, we have formulated and demonstrated a method for constructing well-posed one-way approximations of hyperbolic equations. First, an exact one-way equation is derived for systems that do not vary in *x*. We then construct an efficient approximation of the exact equation based on recursions originally developed for generating nonreflecting boundary conditions. The approximate equations are shown to be well-posed and are able to approximate the exact equations with increasing accuracy as the order of the recursions is increased, provided that the recursion parameters are properly chosen. When the method is applied to *x*-dependent systems, the one-way equation remains well-posed, but physical accuracy is guaranteed only when the variation is sufficiently slow such that leftgoing waves do not significantly modify the evolution of the rightgoing waves. This is not a shortcoming of our formulation, but rather an inherent limitation on the class of problems for which a one-way solution strategy is sensible. Computational cost scaling estimates are derived that explain the improved efficiency of the approximate one-way equations over traditional solution methods.

Next, the method is applied to the linearized Euler equations. A process by which appropriate recursion parameters can be identified is described in detail, which can be used as a guide in the application of the method to other hyperbolic equations. In particular, analytical eigenvalues of the uniform flow Euler equations can be used as a proxy for the eigenvalues of the discretized nonuniform equations for the purpose of parameter selection. The utility of the resulting one-way Euler equations is then demonstrated using three example problems. First, a simple modal problem involving the propagation of monopole acoustic waves is used to verify the convergence of the method. Second, the scattering of acoustic waves by a vortex is calculated. The excellent agreement between the one-way solution and a previous direct-numerical-simulation shows the accuracy of the method, despite the significant *x*-variation of the system. Third, linear wavepackets in a Mach 0.9

jet are computed. Unlike parabolized stability equations, the one-way Euler equations are able to properly capture both the near-field wavepacket and the associated acoustic radiation, which is almost three orders of magnitude less energetic than the nearfield fluctuations. The one-way equations require 34 times less CPU time than a traditional time domain method, highlighting their efficiency.

A limitation of our approximate one-way formulation is that effective recursion parameters can sometimes be difficult to identify. Defining the parameters using the simple strategies discussed in Section 3.2 has proven to be sufficient for a variety of problems, but can sometimes fail due to unexpected behavior of the eigenvalues of $\boldsymbol{M}$. An example related to spurious numerical artifacts was discussed in Section 4.2. Developing robust strategies for overcoming these challenges is an ongoing aspect of our research.

Since our one-way formulation can be applied to any hyperbolic system, it could be a valuable tool for solving a wide range of problems. The most obvious application is to inhomogeneous wave propagation problems that arise in many fields. Examples include underwater acoustics, medical imaging, seismology, and non-isotropic elastic wave problems. One-way equations based on our methodology for these problems could prove to be faster than traditional time domain methods and more accurate than existing one-way equations that are based on factorization and subsequent approximation of quasi-uniform analytical dispersion relations. Additional applications include noise, stability, and transition analysis of free-shear flows such as mixing-layers and jets, as well as wall-bounded flows (for which transverse viscous terms can be incorporated without hindering parabolization) ranging from classical flat-plate boundary layers to complicated swept wings. Unlike the parabolized stability equations, the one-way equations could capture multi-modal behavior within these problems, such as the generation of acoustic waves or interaction between multiple instability modes.

### Acknowledgements

### Appendix A. Generalized one-way equations for systems with singular $\boldsymbol{A}$

In this appendix, we generalize the one-way equations for systems in which $\boldsymbol{A}$ is singular. The essential difference is that, in addition to the usual rightgoing and leftgoing modes, systems with singular $\boldsymbol{A}$ also admit solutions that do not propagate in $x$. These solutions can be thought of either as modes with infinite eigenvalues or as algebraic constraints on the possible behavior of the propagating rightgoing and leftgoing solutions. Well-posed one-way equations can be constructed for these systems based on an extension of Kreiss' theory that was developed by Majda and Osher [38]. The step-by-step development of the generalized one-way equations becomes quite technical, so for brevity we simply state the results.

The exact generalized one-way equation, analogous to equation (22), is

$$\tilde{\boldsymbol{A}}_{++} \frac{d\hat{\boldsymbol{\phi}}_+}{dx} = \boldsymbol{L}_{++}\hat{\boldsymbol{\phi}}_+ + \boldsymbol{L}_{+0}\hat{\boldsymbol{\phi}}_0 + \boldsymbol{L}_{+-}\hat{\boldsymbol{\phi}}_-, \tag{A.1a}$$

$$\boldsymbol{0} = \boldsymbol{L}_{0+}\hat{\boldsymbol{\phi}}_+ + \boldsymbol{L}_{00}\hat{\boldsymbol{\phi}}_0 + \boldsymbol{L}_{0-}\hat{\boldsymbol{\phi}}_-, \tag{A.1b}$$

$$\boldsymbol{0} = \boldsymbol{U}_{-+}\hat{\boldsymbol{\phi}}_+ + \boldsymbol{U}_{-0}\hat{\boldsymbol{\phi}}_0 + \boldsymbol{U}_{--}\hat{\boldsymbol{\phi}}_-. \tag{A.1c}$$

Here, the characteristic variables have been divided into three parts (rather than two) based on the positive, zero, and negative eigenvalues of $\boldsymbol{A}$. The positive eigenvalues of $\boldsymbol{A}$ are contained in the diagonal matrix $\tilde{\boldsymbol{A}}_{++}$. The matrices $\boldsymbol{L}_{++}$, etc., are blocks of the matrix $\boldsymbol{L} = -\left(s\boldsymbol{I} + \tilde{\boldsymbol{B}}\right)$. Similarly, the matrices $\boldsymbol{U}_{-+}$, etc., are blocks of a matrix of $\boldsymbol{U} = \boldsymbol{V}^{-1}$, where $\boldsymbol{V}$ contains the right eigenvectors of the generalized eigenvalue problem $\boldsymbol{L}\boldsymbol{V} = \tilde{\boldsymbol{A}}\boldsymbol{V}\boldsymbol{D}$. The blocks of both $\boldsymbol{L}$ and $\boldsymbol{U}$ are partitioned in the same way as in Section 2.1, but with additional blocks associated with $\hat{\boldsymbol{\phi}}_0$. By eliminating $\hat{\boldsymbol{\phi}}_0$ and $\hat{\boldsymbol{\phi}}_-$, it can be shown that equation (A.1) is well-posed and supports the same rightgoing eigenvalues as the original equations.

Following the form of equation (A.1), the approximate generalized one-way equation is

$$\tilde{\boldsymbol{A}}_{++} \frac{d\hat{\boldsymbol{\phi}}_+}{dx} = \boldsymbol{L}_{++}\hat{\boldsymbol{\phi}}_+ + \boldsymbol{L}_{+0}\hat{\boldsymbol{\phi}}_0 + \boldsymbol{L}_{+-}\hat{\boldsymbol{\phi}}_-, \tag{A.2a}$$

$$\boldsymbol{0} = \boldsymbol{L}_{0+}\hat{\boldsymbol{\phi}}_+ + \boldsymbol{L}_{00}\hat{\boldsymbol{\phi}}_0 + \boldsymbol{L}_{0-}\hat{\boldsymbol{\phi}}_-, \tag{A.2b}$$

$$\left(\boldsymbol{L} - i\beta_+^j\tilde{\boldsymbol{A}}\right)\hat{\boldsymbol{\phi}}^j = \left(\boldsymbol{L} - i\beta_-^j\tilde{\boldsymbol{A}}\right)\hat{\boldsymbol{\phi}}^{j+1} \qquad j = 0, \ldots, N_\beta - 1, \tag{A.2c}$$

$$\hat{\boldsymbol{\phi}}_-^{N_\beta} = 0. \tag{A.2d}$$

Equation (A.2a) has the same convergence properties as equation (25). The recursion parameters should be chosen based on the rightgoing and leftgoing eigenvalues of the generalized system – the infinite eigenvalues associated with the non-propagating solutions can be ignored.

## Appendix B. Special cases associated with pathological properties of $M$

In this appendix, we address some special cases that were omitted from the main text due to assumptions that were made on certain properties of $M$. First, we previously assumed that $M$ is diagonalizable. In general, there is no reason that this must be the case. However, it is always true for some sufficiently large $\eta$, since $M$ tends to a diagonal matrix in this limit. Therefore, the potential for a defective $M$ at some finite value of $\eta$ effects neither the identification of rightgoing and leftgoing eigenvalues nor the well-posedness of the exact or approximate one-way equations.

One the other hand, the convergence proof of the approximate one-way equation at a fixed real frequency depended on the diagonalizability of $M$ at that frequency. Specifically, the eigen-decomposition of $M$ was used in equations (26)–(31) to derive the reflection coefficient $R$, which governs the convergence of the approximate one-way equations. When $M$ is defective, the reflection coefficient can be derived using the Jordan-decomposition of $M$, which always exists, rather than the eigen-decomposition. The derivation follows the same basic steps, with the essential difference being that expansion coefficients associated with the same Jordan block remain coupled. Ultimately, each entry of $R$ takes the form

$$\boldsymbol{r}_{mn} = \frac{\mathcal{F}(\alpha_{+,m})}{\mathcal{F}(\alpha_{+,n})}\, \tilde{\boldsymbol{w}}_{nm}. \tag{B.1}$$

This is exactly the same form as before, except that the modified weights $\tilde{\boldsymbol{w}}_{mn}$ are not constants, but instead depend on the recursion parameters, the order of the recursion, and the specifics of the Jordan form of $M$. Most importantly, the modified weights can grow like $N_\beta^{2(h-1)}$ to leading order, where $h$ is the size of the largest Jordan block. This algebraic growth works against the goal of forcing every $\boldsymbol{r}_{nm}$ to zero, but does not prevent it since the fractional term in equation (B.1) usually exhibits spectral convergence and can always be made arbitrarily small at finite order, as discussed in Section 2.3. Therefore, the approximate one-way equations converge to the exact one-way equation even when $M$ is defective at the frequency of interest.

Second, we assumed in the main text that $U_{++}$, $U_{--}$, $V_{++}$, and $V_{--}$ are full-rank for all $\eta \geq 0$. These matrices are always full-rank when $\eta$ is taken to be sufficiently large since $M$ tends to a diagonal matrix. Therefore, violation of this assumption does not effect the identification of rightgoing and leftgoing solutions or the subsequent statement of a well-posed one-way equation in terms of $\boldsymbol{\psi}$.

However, when one or more of these matrices is singular at a particular frequency, the one-way equation cannot be written in terms of the characteristic variables $\hat{\boldsymbol{\phi}}$ at that frequency. In other words, equation (22) does not follow from equation (21). This is the case because expressing the differential equation for $\boldsymbol{\psi}_+$ and the algebraic condition for $\boldsymbol{\psi}_-$ as a differential–algebraic equation with $\hat{\boldsymbol{\phi}}_+$ as the differential variable and $\hat{\boldsymbol{\phi}}_-$ as the algebraic variable requires that $\hat{\boldsymbol{\phi}}_+$ depends on all of the components of $\boldsymbol{\psi}_+$ and that $\hat{\boldsymbol{\phi}}_-$ depends on all of the components of $\boldsymbol{\psi}_-$. This is only the case if the matrices under consideration are full-rank.

Although in principle this constitutes a real and unpredictable limitation on our one-way formulation, we wish to emphasize that we have never encountered this problem in practice. The singularity of these matrices is easy to detect since it necessarily leads to singularity of the matrix system that is solved numerically to satisfy the recursions.

## References

[1] D. Lee, A. Pierce, E. Shang, Parabolic equation development in the twentieth century, J. Comput. Acoust. 8 (4) (2000) 527–637.
[2] F. Tappert, Ch. The parabolic approximation method, in: Wave Propagation and Underwater Acoustics, in: Lecture Notes in Physics, vol. 70, Springer, New York, 1977.
[3] J. Claerbout, Coarse grid calculation of waves in inhomogeneous media with application to delineation of complicated seismic structure, Geophysics 35 (1970) 407–418.
[4] L. Trefethen, L. Halpern, Well-posedness of one-way wave equations and absorbing boundary conditions, Math. Comput. 47 (176) (1986) 421–435.
[5] L. Halpern, L. Trefethen, Wide-angle one-way wave equations, J. Acoust. Soc. Am. 4 (1988) 890–901.
[6] J. Claerbout, Fundamentals of Geophysical Data Processing, McGraw-Hill, New York, 1976.
[7] J. Claerbout, Imaging the Earth's Interior, Blackwell Scientific Publications, Inc., Cambridge, MA, USA, 1985.
[8] M. Collins, Applications and time-domain solution of higher-order parabolic equations in underwater acoustics, J. Acoust. Soc. Am. 86 (3) (1989) 1097–1102.
[9] F. Jensen, W. Kuperman, M. Porter, H. Schmidt, Computational Ocean Acoustics, Modern Acoustics and Signal Processing, 2001.
[10] B. Engquist, A. Majda, Absorbing boundary conditions for the numerical simulation of waves, Math. Comput. 31 (139) (1977) 629–651.
[11] D. Givoli, High-order local non-reflecting boundary conditions: a review, Wave Motion 39 (4) (2004) 319–326.
[12] M. Guddati, Arbitrarily wide-angle wave equations for complex media, Comput. Methods Appl. Mech. Eng. 195 (2006) 65–93.
[13] T. Herbert, Parabolized stability equations, Annu. Rev. Fluid Mech. 29 (1997) 245–283.
[14] F. Li, M. Malik, On the nature of PSE approximation, Theor. Comput. Fluid Dyn. 8 (1996) 253–273.
[15] P. Andersson, D. Henningson, A. Hanifi, On a stabilization procedure for the parabolic stability equations, J. Eng. Mech. 33 (1998) 311–332.
[16] J. Korte, An explicit upwind algorithm for solving the parabolized Navier–Stokes equations, NASA Technical Paper 3050, 1991, pp. 890–901.
[17] S. Rubin, J. Tannehill, Parabolized/reduced Navier–Stokes computational techniques, Annu. Rev. Fluid Mech. 24 (1992) 117–144.
[18] R.J. Briggs, Electron–Stream Interactions with Plasmas, MIT Press, Cambridge, Massachusetts, 1964.
[19] H. Kreiss, Initial boundary value problems for hyperbolic systems, Commun. Pure Appl. Math. 23 (1970) 277–298.
[20] D. Givoli, B. Neta, High-order nonreflecting boundary scheme for time-dependent waves, J. Comput. Phys. 186 (2003) 24–46.
[21] T. Hagstrom, T. Warburton, A new auxiliary variable formulation of high-order local radiation boundary conditions: corner compatibility conditions and extensions to first-order systems, Wave Motion 39 (2004) 890–901.

[22] T. Hagstrom, T. Warburton, Complete radiation boundary conditions: minimizing the long time error growth of local methods, SIAM J. Numer. Anal. 47 (2009) 3678–3704.
[23] T. Hagstrom, T. Warburton, D. Givoli, Radiation boundary conditions for time-dependent waves based on complete plane wave expansions, J. Comput. Appl. Math. 45 (4) (2007) 1988–1995.
[24] T. Hagstrom, E. Becache, D. Givoli, K. Stein, Complete radiation boundary conditions for convective waves, Commun. Comput. Phys. 11 (2) (2012) 610–628.
[25] K. Mattsson, J. Nordström, Summation by parts operators for finite difference approximations of second derivatives, J. Comput. Phys. 199 (2) (2004) 503–540.
[26] D. Appelo, T. Colonius, A high-order super-grid-scale absorbing layer and its application to linear hyperbolic systems, J. Comput. Phys. 228 (11) (2009) 4200–4217.
[27] K.W. Thompson, Time dependent boundary conditions for hyperbolic systems, J. Comput. Phys. 68 (1987) 1–24.
[28] K. Mohseni, T. Colonius, Numerical treatment of polar coordinate singularities, J. Comput. Phys. 157 (2) (2000) 787–795.
[29] E. Hairer, G. Wanner, Solving Ordinary Differential Equations II: Stiff and Differential–Algebraic Problems, Springer-Verlag, New York, 1971.
[30] S. Candel, Numerical solution of wave scattering problems in the parabolic approximation, J. Fluid Mech. 90 (1979) 465–507.
[31] T. Colonius, S. Lele, P. Moin, The scattering of sound waves by a vortex: numerical simulations and analytical solutions, J. Fluid Mech. 260 (1994) 271–298.
[32] P. Jordan, T. Colonius, Wave packets and turbulent jet noise, Annu. Rev. Fluid Mech. 45 (2013) 173–195.
[33] G.A. Brès, P. Jordan, T. Colonius, M.L. Rallic, V. Jaunet, S.K. Lele, Large eddy simulation of a turbulent Mach 0.9 jet, Tech. rep., in: Proceedings of the Center for Turbulence Research Summer Program, 2014.
[34] G.A. Brès, J. Jaunet, M. Le Rallic, P. Jordan, T. Colonius, S.K. Lele, Large eddy simulation for jet noise: the importance of getting the boundary layer right, in: 21st AIAA/CEAS Aeroacoustics Conference, 2015.
[35] K. Gudmundsson, T. Colonius, Instability wave models for the near-filed fluctuations of turbulent jets, J. Fluid Mech. 689 (2011) 97–128.
[36] A. Sinha, D. Rodriguez, G. Bres, T. Colonius, Wavepacket models for supersonic jet noise, J. Fluid Mech. 742 (2014) 71–95.
[37] P. Jordan, T. Colonius, G.A. Brès, M. Zhang, A. Towne, S.K. Lele, Modeling intermittent wavepackets and their radiated sound in a turbulent jet, Tech. rep., in: Proceedings of the Center for Turbulence Research Summer Program, 2014.
[38] A. Majda, S. Osher, Initial-boundary value problems for hyperbolic equations with uniformly characteristic boundary, Commun. Pure Appl. Math. 28 (5) (1975) 607–675.